Hans-Georg Scherneck et al.: Ocean Tide and Atmospheric Loading, IVS 2002 General Meeting Proceedings, p.205–214
http://ivscc.gsfc.nasa.gov/publications/gm2002/scherneck

Ocean Tide and Atmospheric Loading

Hans-Georg Scherneck [1], *Machiel S. Bos* [2]

[1)] *Chalmers/Radio and Space Science*
[2)] *Delft Institute for Earth-Oriented Space Research (DEOS)*
Contact author: Hans-Georg Scherneck, e-mail: hgs@oso.chalmers.se

Abstract

We describe the ingredients of an automatic service for the dissemination of ocean tide loading coefficients and the considerations that led to the solution employed. The paper reviews the surface loading problem, methods for computation and especially the improvement of coastline resolution for accurate representation of coastal loads. We finally compare the loading results based on several ocean tide models with coefficients estimated from VLBI observations.

1. Introduction

Loading processes are still gaining increasing attention in space geodesy. The resolution of VLBI, using the data bases collected since the late 70s, makes estimation of tidal parameters feasible at the sub-millimeter level. The loading process affects in the first case the station position. This parameter, however, would average out the loading effect in the long-term average. Actually more relevant in this context are the major products of VLBI, Earth Orientation Parameters and, with increasing importance, atmosphere parameters. VLBI is heading towards near-real-time and high-rate applications, like EOP on the ten-minute basis, and atmospheres in a similar pace. On the sub-diurnal time scale, tide processes do generally not average out. Also, one of the findings of GPS in applications to atmospheres is that the zenith delay is sensitive to unmodeled vertical motion. The two processes, loading displacement and wave propagation, can be separated [5], but the correlation of the estimated parameters remains high. In relation to EOP's from small VLBI networks, an ocean-loading induced bias due to horizontal parameters may occur. A study using the VLBI observations from the CONT-94 experiment showed that the admittance of local, incoherent horizontal motion may be several times larger in the case of real data compared to the orientation changes that would be obtained on theoretical grounds using Helmert rotations [24].

The purpose of this paper is to respond to the demands of the analysts in space geodesy to retrieve high-accuracy coefficients for an ocean tide loading model in a convenient way. We describe an automatic ocean loading provider that we have made available on the Internet. We motivate the specific methods of computation that are employed. In the section on VLBI data analysis we show that the different ocean tide models that can be employed to compute the loading coefficients are uncritical at present given the accuracy of the observations.

The process of atmospheric loading is similar as far as the physical effects of load induced deformations of the solid earth body and subsequent displacement of points on the surface are concerned. There is one important difference though. Tidal processes are described to a very high order of approximation by sinusoidal variations in time. It turns out that only a few coefficients need to be imported into fairly unsophisticated formulas in order to describe tidal motion during extensive time periods. The atmospheric pressure, however, is aperiodic in most of its signal power.

Therefore, time series of loading displacements must be computed for each station at subdiurnal intervals. Generally, ocean loading tide and atmospheric pressure induced deformations are similar in size. The former is of course more pronounced in oceanic and coastal areas, whereas atmospheric loading is more efficient in the interior of continents, where there is no ocean to yield and equilibrate the surface pressure. In the ocean, the inverse barometer response is widely efficient, but limitations have recently been pointed out [15].

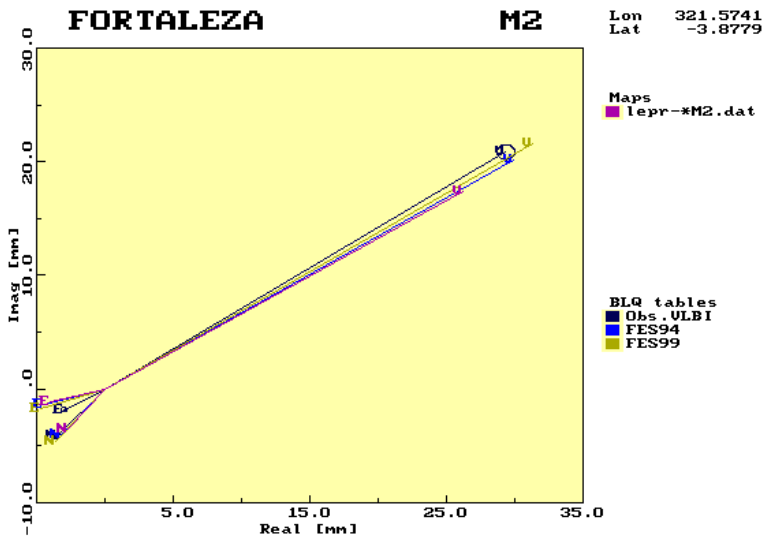

Figure 1. Loading phasors at Fortaleza, tide M_2. Vertical motion is indicated by symbol V, east and north by E and N, respectively. The FES94 model [13] has been used in the map mode of load computations, equation (7), shown in dark gray (purple), and using the point load method with refined coastlines, shown in lighter gray (blue). The difference in the vertical component is five millimeters. Agreement between the point load results based on [13], the more recent 0.25°model [11] (lightest gray (green)), and VLBI observations shown in black with one-sigma error ellipse (see section 4 for details) is much better, hinting at a lesser reliability of the map method.

2. Methods of Computation

The loading effect on a radially symmetric earth can be computed by convolution of the surface mass load with a kernel function, the Green's function of the normal stress surface loading problem on a self-gravitating planet. The property of radial symmetry of the structure and rheology renders the Green's function to depend only on the distance between the load point and the field point, not on the explicit location or on the azimuth.

The Green's functions are computed from solving the loading problem for each spherical harmonic degree at a time, giving three independent parameters at each degree n, the so-called load Love numbers (LLN). These three dimensionless numbers, h'_n, l'_n, and k'_n characterize the vertical displacement u, the horizontal displacement $\mathbf{v}$, and the secondary gravity potential perturbation Φ, respectively. All other loading effects (like surface gravity change δg, tilt, vertical deflection,

strain) can be represented by linear combinations of the LLN.

We thus have the point-load (PL) Green's functions and the relations between a loading mass element dm and the incremental effect it generates as follows

$$du = \frac{a}{M_E} \sum_{n=0}^{\infty} h'_n P_n(\cos\theta)\, dm \tag{1}$$

$$d\Psi = \frac{a^2}{M_E} \sum_{n=0}^{\infty} l'_n P_n(\cos\theta)\, dm \tag{2}$$

$$\mathbf{v} = -\nabla\Psi = \hat{\alpha} \sum_{n=0}^{\infty} l'_n \frac{dP_n(\cos\theta)}{d\theta}\, dm \tag{3}$$

$$d\Phi = \frac{ga}{M_E} \sum_{n=0}^{\infty} k'_n P_n(\cos\ \theta)\, dm \tag{4}$$

$$\delta g = \frac{2g}{a} u + \frac{g}{M_E} \sum_{n=0}^{\infty} \left(n\ -\ (n-1)\ k'_n\right) P_n(\cos\ \theta)\, dm \tag{5}$$

where a, g, and M_E denote the radius, gravity and mass of the model earth, respectively (one uses the mean values of the ellipsoidal quantities). Note that ψ is a horizontal displacement potential, a scalar quantity. The Green's functions involve Legendre polynomials P_n. The distance θ is measured as an angle along a great circle, and the azimuth is $\hat{\alpha}$. The sums can generally not be truncated; limiting values can be computed with the Kummer transform [8], [22].

An identity of the above using spherical harmonic development (SHD) provides

$$\left\{ \begin{array}{c} U_{nmk} \\ \Psi_{nmk} \end{array} \right\} = \frac{3}{2n+1} \frac{\rho}{\bar{\rho}} \left\{ \begin{array}{c} h'_n \\ l'_n \end{array} \right\} \zeta_{nmk} \tag{6}$$

for the displacement scalars, where, instead of the loading mass, we have developed the ocean tide amplitude ζ, and multiplied with a constant ocean water density, ρ. The earth's mean density is denoted by $\bar{\rho}$.

The maximum degree of an SHD is limited in practice. Therefore, the following advantages and disadvantages are encountered in the PL method (equations (1) to (5)) and the SHD (equation (6). The SHD would calculate an entire global map for each partial tide and component of the loading effect in one stage. This appears rather convenient contemplating the ever increasing number of stations demanding a continuing service for employing the PL integral method.

In practice, the PL integral is replaced by a sum over the grid elements of an ocean tide model. The ocean grid can be refined according to convergence criteria. The requirement for refinement occurs when a station is near a coast, since the Green's functions have a singularity at zero distance (the asymptote is one over the chord distance).

If crude accuracy is sufficient, the SHD method can be used. Experience shows that errors in excess of 1 mm result at many coasts, so the method is not an option for VLBI. The reason for the inaccuracy is related to the coarse resolution of the coasts, rather than to the truncation implied by the low maximum SH degree of the LLN included in (6). In an attempt to increase the accuracy by extending the degree range of the harmonic development, a semi-fast method can be used that utilizes the circular convolution theorem of Fourier series ($\mathcal{F}$ denoting the discrete Fourier transform). It proceeds by taking all grid nodes along a pair of colatitude rings (β_k,β_l)

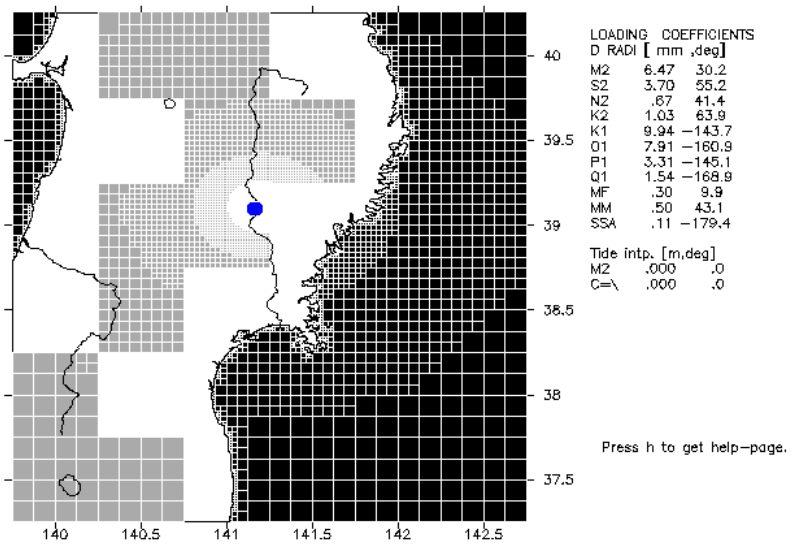

Figure 2. The refined loading grid. Inside a 3°×3°area, the coastline is retrieved using a quad-tree algorithm. The basic box size for load integration is refined by an areal factor of four when the distance to the site is less than ten times the radius of a box or until it fits the coastline. The distance-dependent refinement is seen in the figure in the case of the land-boxes (gray). The example is for Mizusawa, Japan.

into account simultaneously

$$\mathcal{F}\{\mathbf{u}_k\} = \frac{a^3\rho}{M_E}\,\mathcal{F}\left\{\tilde{\mathbf{G}}_{kl}\right\}\mathcal{F}\{\zeta_l\} \tag{7}$$

where we use a box-integrated Green's function

$$\tilde{\mathbf{G}}_{kl} = \left[\tilde{\mathcal{G}}_{kl,0},\ \tilde{\mathcal{G}}_{kl,1},\ \ldots,\ \tilde{\mathcal{G}}_{kl,M-1}\right]$$

$$\tilde{\mathcal{G}}_{kl,r} = \int_{\beta_l-\Delta\beta/2}^{\beta_l+\Delta\beta/2}\int_{(r-1/2)\Delta\lambda}^{(r+1/2)\Delta\lambda} \mathcal{G}(\cos\beta_k\cos\beta + \sin\beta_k\sin\beta\cos\lambda)\cos\beta\; d\beta\; d\lambda$$

The formulas for the horizontal displacement potential follow analogously, and $\mathcal{G}$, the Green's function, is the infinite sum in (1) or (2), respectively.

Thus, this semi-fast map method with the integrated Green's function treats effectively the ocean tide on its original grid. It does the equivalent of distributing a tide value constantly over a grid box and convolving it with the point-load Green's function. This extension alleviates the LLN truncation; however the coastline cannot be refined without refining the grid everywhere globally. Going to the 5'×5' grid of a standard topographic data base to retrieve a more accurate coastline would result in enormous computation times. Using the 0.5°×0.5° of [13] we arrive at errors in excess of 1 mm for example at Fortaleza (Fig. 1). Thus we are doubtful about the fast or semi-fast methods that generate loading results on global maps.

We rather stay with a per-site PL computation. In the following section we describe an automatic service available over the Internet.

3. The Automatic Ocean Loading Provider

The automatic ocean loading provider is a web service available at `http://www.oso.chalmers.se/~loading`. We employ the point-load method, one set of Green's functions for a continental earth structure, and eleven different ocean tide models. The different models reflect the most important source of uncertainty in the model computations at present.

3.1. Ocean Tide Models

The ocean tide models can be divided into those which are purely hydrodynamic, purely based on altimetry data and those which are of a hybrid form. Nowadays, most published models are of the last type. All models described are barotropic (depth-averaged) and employ the Laplace tidal equations. Regularly, these models are self-gravitating and self-loading using a local coefficient [1], a procedure which, however, may yield significant systematic error [21].

One of the first accurate ocean tide models was the one of Schwiderski [27]. Its success was partly the result of forcing the model to fit almost all available tide gauge observations at the coast. For long-term continuity it has again been added to the ocean tide loading provider. A closely related model is NAO99 [16] but with the inclusion of altimetry data and an improved assimilation scheme. FES94.1 [13] is a purely hydrodynamic finite-element model with enhanced resolution on the shelves. FES95.2 [14] was an update of FES94.1 with the introduction of better Arctic tides and a longwave adjustment using TOPEX/Poseidon (T/P) altimetry data.

Other models which also employ a longwave T/P adjustment of and loading effects due to FES94.1 are CSR3.0, CSR4.0 [6] and GOT99.2b [20]. Since T/P does not exceed the $\pm 66°$ latitude bounds, these models are equal to FES94.1 in these polar regions. Furthermore, CSR3.0 and CSR4.0 have spurious wet nodes on land. These must be carefully excluded in loading calculations. Secondly, these two models do not extend under the Antarctic ice shelves. To amend this, the values of GOT00.2 have been added in these places. GOT00.2 is an update of GOT99.2b and has been extended by the assimilation of ERS1/2 altimetry data.

Recently, the models FES98 [11] and FES99 [12] have been published. They are both hydrodynamic models with assimilated tide gauge, while FES99 also incorporates T/P data. Finally, the model TPXO.5 [7] has been added because it is an independent model; it is a fully inverse, hydrodynamic model that uses the representer method to fit tide gauge and altimetry data.

All models are given on a $0.5° \times 0.5°$ grid except for Schwiderski which has $1° \times 1°$ and FES98/99 which are given on a $0.25° \times 0.25°$ grid.

It must be noted that these models do not conserve the water mass during one tidal cycle. To remedy this defect it is common practice to subtract a uniform layer with a certain phase lag from the model. Fortunately this effect is small for the most recent ocean tide models.

3.2. Implementation

For the computation of the loading using the PL method, the integral must be replaced by a summation. A natural choice of the discretization is to use the grid of the ocean tide model and sum each cell that has tidal values weighted with the Green's function. Thus:

$$du(\mathbf{r}) = \rho \sum_{i=1}^{N} \sum_{j=1}^{M} \mathcal{G}\left(|\mathbf{r} - \mathbf{r'}_{ij}|\right)\ \zeta_{ij}\ \Delta A_{ij} \tag{8}$$

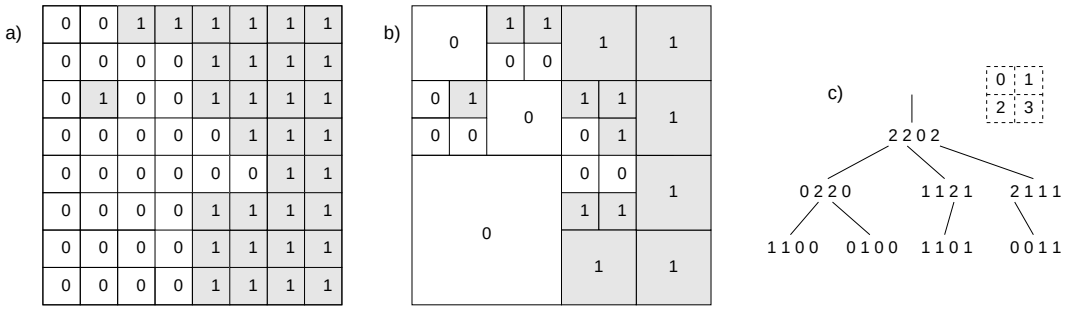

Figure 3. The schematic principle of the quad tree. First, the coastline data of GMT is digitized (a). Next, the data is decomposed into blocks (b) and finally these blocks are stored into a hierarchical tree (c). In this three, the highest level represent the whole area, one level down the leaves describe the status of the 4 smaller parts of the area. The number 2 indicates that the area contains land and water, the number 1 that it is totally land and 0 that it is totally filled with water. The nodes at each branch describe, from left to right, the upper-left, upper-right, bottom-left, bottom-right part of the cell.

with N and M the number of rows and columns of the grid. For the density of water we assume ρ=1030 kg/m^3. The Green's function is available in tabular form [8], [9]. The use of point loads to represent the effect of an areal load $\rho\zeta\ \Delta A$ is justified for large distances. For distances less than ten times a grid cell diameter, however, this is no longer valid. Furthermore, when fitting the model to the coastline it becomes important to represent the actual amount of water loading the Earth. The solution is to refine the grid, and this can be done gradually and locally around the station where it is needed. Inside the refinement area, the tide variation inside a gridbox can be interpolated or extrapolated into e.g. estuaries using the neighboring nodes. By doing the refinement automatically most of the arguments against this method [18] are removed.

The refinement is performed by dividing a grid cell recursively into 4 smaller blocks until two criteria for 1) approximating the cell load by a point load and 2) fit of the model to the coastline are satisfied. The tidal values for these smaller blocks are derived using bilinear interpolation of the original model.

Finally one has to define the water area A. For high coastline resolutions of less than $1km$ the size of a global digitized land-water map becomes prohibitive. In cooperation with Simon Williams [*pers. communication, 2000*] a compression program was developed, again exploiting the algorithm of recursively divided blocks. First, the coastline data base of GMT [28] has been digitized (resolution=0.00549°$\approx 600m$) after which the data has been decomposed into a quad tree [10], see Figure 3.

In practice Equation 8 is computed first with a program called `olfg` [23]. If necessary, a square of $3^\circ \times 3^\circ$ is left out of the computation and post-processed with the program `olmpp`. A screenshot of such an area is given in Figure 2.

3.3. Comparison of Program Codes

Other programs that compute the ocean tide loading using the PL method are: `NLOADF` [2], `GOTIC2` [17], `conmodb` [*Baker, pers. comm. 2000*] and `LOADSDP` [19]. `NLOADF` differs from the others by projecting the ocean onto a template grid centered on the station, each ring having approximately constant loading sensitivity. The highest coastline resolution is $1/64^\circ \approx 1.7km$.

Table 1. The vertical ocean loading tide computed by different programs using CSR4.0, harmonic M_2 [6]. LOADSDP uses FES95.2 [14] and a regional model for Canadian waters, however [19]. The displacement is positive upwards and the phase lags negative relative to the astronomical tide at Greenwich.

	NLOADF [2]		GOTIC2 [17]		conmodb [4]		LOADSDP [19]		olfg/olmpp [23]	
Station	mm	°	mm	°	mm	°	mm	°	mm	°
FD-VLBA	1.48	168.4	1.46	168.7	1.45	167.8	1.43	165.2	1.48	167.7
Fortaleza	35.84	34.1	36.20	34.0	35.56	33.8	35.55	34.0	35.70	34.0
GilCreek	8.97	99.5	9.08	99.4	8.95	99.2	8.99	97.4	9.05	99.2
HartRAO	16.53	-131.9	16.54	-131.9	16.47	-131.9	16.42	-131.3	16.66	-131.8
Kashima	8.87	46.2	8.91	46.1	8.87	46.5	8.80	44.5	8.80	46.2
Kokee	12.63	-120.3	12.79	-120.7	12.58	-120.2	12.55	-119.2	12.63	-120.0
DSS65	14.36	-89.0	14.51	-89.2	14.35	-89.2	14.64	-89.4	14.55	-89.2
Medicina	5.33	-70.9	5.31	-71.0	5.25	-70.4	5.49	-70.4	5.43	-71.3
Noto	5.93	-85.4	5.93	-85.2	5.93	-85.6	5.93	-85.3	6.03	-85.7
Ny-Alesund	8.14	174.0	8.39	174.5	8.22	173.7	7.86	-175.9	8.37	174.1
Onsala	3.48	-67.0	3.42	-66.1	3.47	-64.7	3.60	-69.2	3.51	-65.4
Richmond	7.74	162.7	7.80	162.7	7.63	162.3	8.27	170.0	7.81	162.0
Westford	7.45	-179.1	7.56	-179.2	7.49	-179.3	8.24	157.3	7.31	-179.2
Wettzell	5.08	-71.5	5.05	-72.0	5.02	-71.5	5.29	-71.7	5.08	-71.5

Table 2. Formal uncertainties of estimated load tide coefficients in this study. The unit is millimeters.

Station	vert.	horiz.	Station	vert.	horiz.	Station	vert.	horiz.
FD-VLBA	0.34	0.09	Fortaleza	0.65	0.20	Gilmore	0.24	0.08
HartRAO	1.05	0.32	Kashima	1.01	0.31	Kokee	0.34	0.12
DSS65	1.03	0.26	Medicina	0.77	0.18	Noto	1.30	0.29
Ny-Ålesund	0.48	0.14	Onsala	0.48	0.14	Richmond	0.56	0.13
Westford	0.24	0.08	Wettzell	0.27	0.10			

GOTIC2 uses integrated Green's function and has a manual high-resolution land masking feature. LOADSPD is also a direct implementation of Equation 8 using FES95.2 and several local ocean tide models.

As these independent programs use the same input (CSR4.0, in the Antarctic region augmented with GOT00.2) and the same Green's functions (Gutenberg-Bullen Earth), they can be employed to indicate the numerical accuracy of loading coefficients.

The results are listed in Table 1. One can see, excluding LOADSDP because it uses another model, that the differences are small and the numerical accuracy is seen to be near $0.2mm$. The effect of using another Green's function such as PREM [3] is around $0.1mm$ and is therefore negligible.

4. VLBI Observations and Discussion

We use estimated ocean loading coefficients from the VLBI solution reported in [26]. Table 2 shows the uncertainties for each station. The uncertainties vary as a result of signal power and number of experiments.

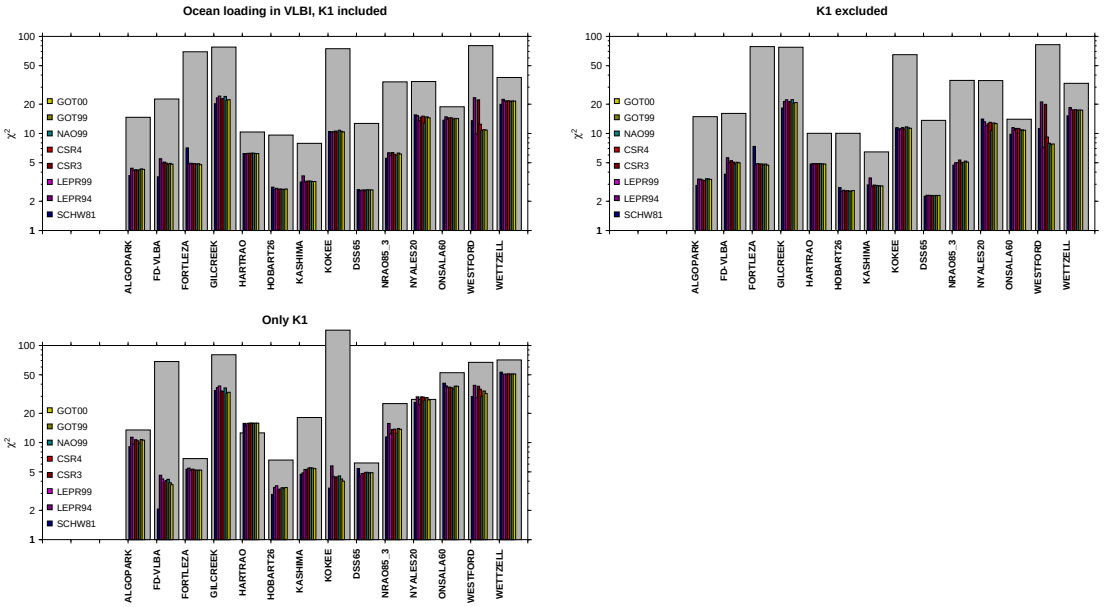

Figure 4. Comparison of observed ocean loading tide coefficients with models. Shown is the weighted Chi-square of the fit, including the eight diurnal tides and the three spatial components. The wide, gray bars show the observed signal in terms of multiples of the standard deviation, and the coloured bars show the remaining signal after subtracting one of the seven tide loading models. The problems with the K1 tide in the observations are exhibited by excluding this tide in the middle frame, and showing it separately in the lower frame.

In the comparison with models we show

$$\chi^2 = \frac{1}{3N} \sum_{n=1}^{N} \sum_{c=1}^{3} \frac{\left| S_{nc}^{(o)} - S_{nc}^{(m)} \right|^2}{\sigma_{nc}^2}$$

where S_{nc} denotes a complex valued loading coefficient, superscript (o) the VLBI observation, n steps through the tides (M_2, S_2, N_2, K_2, K_1, O_1, P_1, Q_1), and c counts the three spatial components. The result is shown in Figure 3. The different tide models we have included, signified by superscript (m), are the Naval Surface Weapons Center model, SCHW81 [27]; two versions of the Grenoble/CNES model, LEPR94 [13] and LEPR99 [11]; two versions of the University of Texas Center of Space Research model, CSR3 and CSR4 [6]; two versions of the Goddard Space Flight Center model, GOT99 and GOT00 [20]; and the model from the National Astronomical Observatory of Japan, NAO99 [16].

The most noticeable result of the comparison is that the internal agreement among the models is much greater than between any single model and our VLBI observations. The variation between the models at Westford is due to the Gulf of Maine, which is present in SCHW81, CSR4, LEPR99, GOT99–00, and NAO99, but excluded in the other models. The K_1 tide is observed in good agreement with the ocean loading model only at two stations, Fort Davis (FD-VLBA) and Kokee Park. In all other cases the models do not explain more than 50 percent of the observed tide. Both Fort Davis and Kokee Park have considerable diurnal solid earth tides; problems with that tide would affect all stations except eventually one at the equator (where the vertical and east

components are zero) or at 45° (where the north component is zero). Closer inspection shows that errors at K_1 exist likewise in the vertical and the horizontal components.

We know from [24] that the vertical component decouples almost perfectly from the Earth Orientation parameters. Supposing a common source for the defect, one has to look into station-dependent conditions. The question arises why the results seem to have much less systematic error at Fort Davis and Kokee.

Onsala shows the greatest disagreement. Problems with the modelling code or with ocean models are not very likely, however, since GPS solutions appear to be in quite good agreement with models [25]. From discussions with Leonid Petrov [*pers. comm., 2002*] we realize that our VLBI solution appears to contain more systematic error power than a recent GSFC solution. There is a lot more to explore here.

5. Conclusions

Ocean tide loading modelling appears to provide consistent results. We have compared different software products and a range of different ocean tide models. A predominant error source appears to exist at the K_1 tide frequency. The perturbation could be an effect of solar radiation, which leaks into the K_1 frequency band.

It appears advisable to recompute ocean loading estimates from VLBI, including the experiments after 1999 and take a careful look at possible sources of perturbations, in particular in the diurnal frequency band.

Acknowledgments. We thank Rüdiger Haas for making the VLBI results available to us. The contributors of ocean loading modelling code and the makers of global ocean tides are kindly acknowledged. This work is supported by grants from the Swedish Research Council and by the European Union program for Training and Mobility of Researchers.

References

[1] Accad, Y. and Pekeris, C. L., Solution of the tidal equations for the M_2 and S_2 tides in the world oceans from a knowledge of the tidal potential alone, Phil. Trans. Roy. Soc. London, Ser. A, Vol.290, 235–266, 1978.

[2] Agnew, D.C., NLOADF: a program for computing ocean-tide loading, J. Geophys. Res., Vol.102, 5109–5110, 1997.

[3] Anderson, D.L., and Dziewonski, A., Preliminary Reference Earth Model, Phys. Earth. Planet. Int., Vol. 25, 297–356, 1981.

[4] Baker, T.F. Tidal gravity in Britain, tidal loading and the spatial distribution of the marine tide, Geophys. J. R. astr. Soc., Vol. 62, 249–267, 1980.

[5] Dach, R., R. Dietrich, Influence of the ocean loading effect on GPS derived precipitable water vapor, Geophys. Res. Letters, Vol. 27, 2953–2956, 2000.

[6] Eanes, R. and S. Bettadpur, The CSR 3.0 global ocean tide model, Center for Space Research, Technical Memorandum, CSR-TM-96-05, 25pp., 1996.

[7] Egbert, G. D., Bennett, A. F., and Foreman, M. G. G. TOPEX/POSEIDON tides estimated using a global inverse model. J. Geophys. Res., Vol.99, 24,821–24,852, 1994.

[8] Farrell, W.E., Deformation of the Earth by Surface Loads, Rev. Geophys. Space Phys., Vol. 10, 761–797, 1972.

[9] Francis, O. and P. Mazzega, Global charts of ocean tide loading effects. J. Geophys. Res., Vol.95, 11,411–11,424, 1990.

[10] Knuth, D. E., Fundamental Algorithms: The art of computer programming, Vol. 1. Addison-Wesley, second edition, 1973.

[11] Lefvre, F., Lyard, F. H., and Le Provost, C. FES98: A new global tide finite element solution independent of altimetry. Geophys. Res. Letters, 27(17):2717-2720, 2000.

[12] Lefèvre, F., Lyard, F. H., Le Provost, C. and Schrama, E. J. O., FES99: A tide finite element solution assimilating tide gauge and altimetric information. J. Atm. Oceano. Tech., *submitted*, 2001.

[13] Le Provost, C., M.L. Genco, F. Lyard, P. Vincent, and P. Canceil, Spectroscopy of the world ocean tides from a finite element hydrological model, J. Geophys. Res., Vol.99, 24,777–24,798, 1994.

[14] Le Provost, C. Lyard, F., Molines, J. M., Genco, M. L. and Rabilloud, F., A hydrodynamic ocean tide model improved by assimilating a satellite altimeter-derived data set, J. Geophys. Res., Vol.103(C3), 5513–5529, 1998.

[15] Mathers, E.L., and P.L. Woodworth, Departures from the local inverse barometer model observed in altimeter and tide gauge data and in a global barotropic numerical model, J. Geophys. Res., Vol.106, 6957–6972, 2001.

[16] Matsumoto, K., Takanezawa, T. and Ooe, M. Ocean Tide Models Developed by Assimilating TOPEX/POSEIDON Altimeter Data into Hydrodynamical Model: A Global Model and a Regional Model Around Japan. J. of Oceanog., Vol.56, 567–581, 2000.

[17] Matsumoto, K., T. Sato, T. Takanezawa, and M. Ooe, GOTIC2: A Program for Computation of Oceanic Tidal Loading Effect, J. Geod. Soc. Japan, Vol.47, 243–248, 2001.

[18] Mitrovica, J. X., Davis, J. L., Shapiro, I. I., A spectral formalism for computing three-dimensional deformations due to surface loads. 1 Theory, J. Geophys. Res., Vol.99, 7057–7073, 1998.

[19] Pagiatakis, S.D.. Program LOADSDP for the calculation of ocean load effects. Manuscripta Geodaetica, Vol.17, 315–320, 1992.

[20] Ray, R., A Global Ocean Tide Model From TOPEX/POSEIDON Altimetry: GOT99.2, NASA Technical Memorandum, NASA/TM-1999-209478, National Aeronautics and Space Administration, Goodard Space Flight Center, Greenbelt, MD, 1999.

[21] Ray, R., Ocean Self-Attraction and Loading in Numerical Tidal Models. Marine Geodesy, Vol.21, 181–192, 1998.

[22] Scherneck, H.-G., Loading Green's functions for a continental shield with a Q-structure for the mantle and density constraints from the geoid, Bull. d'Inform. Mares Terr., Vol. 108, 7775–7792, 1990.

[23] Scherneck, H.-G., A parametrized solid earth tide model and ocean tide loading effects for global geodetic baseline measurements, Geophys. J. Int., Vol.106, 677–694, 1991.

[24] Scherneck, H.-G., R. Haas, Effect of horizontal ocean tide loading on the determination of polar motion and UT1, Geophys. Res. Let., Vol. 26, 501–504, 1999.

[25] Scherneck, H.-G., J.M. Johansson, and F.H. Webb, Ocean Loading Tides in GPS and Rapid Variations of the Frame Origin, in K.-P. Schwarz (ed.): Geodesy beyond 2000 The Challenges of the First Decade, IAG General Assembly Birmingham, July 19-30, 1999, pp. 32–40, 2000.

[26] Scherneck, H.-G., R. Haas, and A. Laudati, Ocean loading tides for, in, and from VLBI, in N.R. Vandenberg and K.D. Baver (eds.): International VLBI Service for Geodesy and Astrometry, 2000 General Meeting Proceedings, pp. 257-262, NASA/CP-2000-209893, NASA Center for AeroSpace Information, Hanover, MD, 2000.

[27] Schwiderski, E. W., On charting global ocean tides, Rev. Geophys. Space Phys., Vol.18, 243–268., 1980.

[28] Wessel, P., Smith, W. H. F., A global, self-consistent, hierarchical, high-resolution shoreline database, J. Geophys. Res., Vol.101, 8741–8743, 1996.